Thermal Science and Engineering Progress 47 (2024) 102304

Contents lists available at ScienceDirect

Thermal Science and Engineering Progress

journal homepage: www.sciencedirect.com/journal/thermal-science-and-engineering-progress

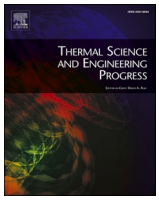

Heat transfer enhancement of a lithium-ion battery cell using vertical and spiral cooling fins

Ali Alzwayi, Manosh C. Paul *

Systems, Power & Energy Research Division, James Watt School of Engineering, University of Glasgow, Glasgow G12 8QQ, UK

ARTICLE INFO

Keywords:
Battery thermal management system
Cooling fins
Spiral fins
Battery temperature
Lithium-ion battery
Computational Modelling

ABSTRACT

Lithium-ion batteries are widely regarded as the primary source of power for electric cars due to their high energy density, long lifespan, and lack of memory effect. However, their efficacy and safety greatly depend on the temperature at which they operate. Therefore, a battery thermal management system (BTMS) is crucial to ensure the safety of an electric vehicle. This research presents a model of a BTMS that employs a single cylindrical lithium-ion with longitudinal and spiral fins on the cell surface to investigate its cooling effectiveness. Effects of the fin's number, rotation, thickness, length, and position are assessed at various current rates. The results show that the fins reduce the maximum cell temperature when compared to a finless case and become more effective at a low Reynolds number. Despite the fact that increasing the number of fins enhances the heat transfer area, when the number of fin reaches more than 3, they become a barrier to the flow around the cell and hence increase the battery temperature. The orientation of the fin also has a significantly impact on the heat transfer between the cell and air cooling, with the cell temperature rising by 1.5 °C when compared to the half-length of a longitudinal fin. However, the cooling benefit is found to be very modest when the half-fin is placed in various locations on the battery surface (i.e., top, middle, and bottom). Furthermore, compared to the longitudinal fins, the spiral fins reduce the cell temperature by 3.2%, resulting in a 65.6% reduction in material usage.

1. Introduction

Global warming is one of the greatest threats facing the modern world, and the transport sector contributes to 24.3% of the total world's CO_2 emissions [1], of which motor vehicles account for a large share [2]. Therefore, adopting electric vehicles (EVs) have the great potential to drastically reduce greenhouse gas emissions.

Batteries are considered one of the essential components of EVs. Lithium-ion batteries (LIBs) are prevalent in EVs because of their high-energy density, long lifespan, and environmental friendliness [3]. However, LIBs generate heat when charging and discharging; and as heat is incapable of being carried from batteries, temperature within a battery pack increases rapidly. A high temperature can significantly affect the battery's thermal performance and lifespan, and a local high temperature can also increase the temperature difference in battery packs, further shortening the cell's service life. Moreover, a heat accumulation in one battery may trigger a series of exothermic chemical reactions, leading to an express increase in battery temperature [4]. Considering variation in ambient temperature in different world regions, LIBs generally operate between −20 and 60 °C [5]. On the other hand, an optimum operating temperature stays between 25 and 50 °C [6–8] and LIBs are electrically connected in series and parallel to form a pack to satisfy the power requirement for an EV. Therefore, uniformity of the cell temperature in battery pack should be maintained as homogeneous as possible and should not exceed 5 °C [9]. To date, various strategies have been implemented for battery thermal management to ensure an optimum operating temperature such as air cooling/heating, liquid cooling/heating, phase change materials (PCM) and a combination of these [10]. A liquid coolant has a high heat transfer coefficient, making it an efficient and compact cooling medium. However, a typical liquid cooling system has a massive and complex structure that requires high investment costs and power consumption [11]. In contrast, air cooling and PCM both have a lower specific heat capacity and a thermal conductivity than a liquid system, resulting in an inefficient process of heat transfer. As a result, cooling fin becomes an effective and simple method to increase the heat removal and simultaneously to reduce the high temperature in a battery pack.

Moreover, PCM is a passive cooling system that utilises its latent heat capacity to restore the heat generated by battery and control its temperature. As PCMs have low thermal conductivity, several studies have been conducted to improve the PCMs' thermal conductivity by attaching

* Corresponding author.
E-mail address: Manosh.Paul@glasgow.ac.uk (M.C. Paul).

https://doi.org/10.1016/j.tsep.2023.102304
Received 21 July 2023; Accepted 22 November 2023
Available online 23 November 2023

Nomenclature

A	equation coefficient
w_f, L_f, t_f	dimensions of fin (m)
u_i	ith component of velocity (m/s)
x_i	ith component of coordinate (m)
C_1, C_2, C_μ	parameters in the k-ε turbulence model
C-rate	Charge and discharge current with respect to its nominal capacity
Cp	specific heat (J/kg)
p	pressure (Pa)
Δp	pressure drops (Pa)
k	turbulent kinetic energy (m^2 /s^2)
h	convective heat transfer coefficient
V	total velocity of air (m/s)
D_h	hydraulic diameter of the duct (m)
Q_T	heat transfer rate (W/m^2)
$\dot{m}$	air mass flow rate (kg/s)
t	time (s)
N	number of fins
T	temperature (°C)
Re	Reynolds number
SOC	state of charge
RE	relative error
PCM	phase change material

Greek symbols

ρ	density (kg/m^3)
ε	dissipation rate of turbulent kinetic energy (m^2/s^3)
δ_k, δ_ε, δ_T	parameters of the k-ε turbulence model
λ	thermal conductivity, (W/m·K)
μ	dynamic viscosity (Pa·s)
φ	heat source intensity (W/m^3)

Subscripts

a	air
b	battery
exp	experimental
num	numerical
t	turbulent

fins on the surface of battery cells [12–17]. Wang et al. [12] suggested using a cylindrical battery with straight vertical fins in a PCM cooling system. They experimentally demonstrated that the best cooling performance of the system is achieved with a total of eight rectangular fins. Huang et al. [13] also reported that the use of fins enhanced the PCM thermal conductivity and thus enlarged the heat exchanger area with a cooling medium. The maximum temperature and its difference for an optimum BTMS reported to decrease by 38.72% and 40.09%, respectively. Lei et al. [14], on the other hand, used aluminium fins and foam to enhance the thermal conductivity of PCM to maintain the battery temperature. In contrast, Zhang et al. [15] investigated another method of adding fins to a liquid cooling channel in a PCM cooling system. It was disclosed that both the battery's maximum and cell temperatures decreased. Ping et al. [16] examined the effect of fin thickness in a PCM battery module. Ramin and Babak [17] analysed the effect of inclination angle on a finned enclosure in a natural convection-driven flow. Another study [18] demonstrated that using fins with PCM in a BTMS could also lower the battery temperature. However, PCM cooling systems have yet to make a breakthrough in EV industry due to their high cost, leaking concerns and stringent structural requirements, and also they need to be regenerated after being completely melted [19,20].

On the other hand, air-cooling systems (ACSs) are mainly applied in light-duty EVs having small-size battery packs [21]. Owing to their simple structure and configuration, low initial and maintenance cost, simple integration and no risk of leakage, it is found to be more favourable compared to PCM and liquid cooling methods [22]. Moreover, ACSs can significantly reduce the battery manufacturing cost, thus directly lowering the price of EVs [18,19]. However, despite its advantages, a poor convective heat transfer coefficient of air often cannot meet the heat dissipation requirement for heavy-duty EVs; also, it is associated with the problem of significant temperature non-uniformity in battery pack [23]. Therefore, heat removal enhancement of a battery is achieved by Zhang et al. [24] using various fin heat sink geometries. The effect of surface anodisation was considered; and inclined interrupted fins with surface anodization provided the best thermal performance compared to other fins' geometries. Notably, the performance increased by 27 % when compared to a typical heat sink because of the enlarged area, resulted in the increased convection heat transfer. A radiator with a bionic surface structure was proposed by Yang et al. [25]. In the study, the maximum temperature and temperature difference were computed for three different types of fins (rectangle, trapezoid and ellipse) with various thickness, height and length. Another study by Chen et al. [26] dealt with a 3D CFD modelling for the detailed cell-level thermal and pressure drop performance of the ACS concept for battery packs. The fin configurations, pin–fin channel, and fin outside design cooling concepts did not satisfy the thermal requirements.

In a subsequent study, four alternative cooling techniques were examined by Chen et al. [27]; and according to their assumptions, a simple air cooling requires more energy than a direct, indirect, and fin cooling. Temperature uniformity of LIBs and maintaining temperature within the acceptable range for efficient operation are addressed by Gao et al. [28], where fins, made of aluminium alloy or graphite sheets, are applied between the prismatic battery cells. Graphite sheet fins provided better temperature uniformity than aluminium alloy fins because of their higher thermal conductivity than aluminium. Mohammadian et al. [29,30] incorporated porous aluminium foams into an air-cooling aluminium pin–fin heat sink. A 70% inner surface coverage of cooling channel with aluminium pin fins and porous aluminium foam insertions was proposed to achieve an ideal temperature uniformity and minimise the maximum temperature. Within the context of ACS, thermal management of a Li-ion battery pack was also studied by Shahabeddin and Yuwen [31], in which a three-dimensional transient thermal analysis consisting a special kind of pin fin heat sink was performed. The effects of pin fins arrangements, discharge rates, inlet airflow velocities, and inlet air temperatures on the battery were investigated. The results showed that the heat sink without pin fins not only decreased the bulk temperature inside the battery, but also reduced the standard deviation of the temperature field inside the battery.

An air-cooled battery module with a thermally conductive heat spreading plate (HSP) was investigated numerically by Yefei et al. [22]. The cylindrical batteries were arranged in 4 × 5 aligned arrays and the HSP was placed at the middle of the batteries. Multi-objective optimization of a double-layer HSP case was conducted including the thickness, length of sleeve tube, downstream length of HSP, and spacing of the adjacent battery cells. Both the temperature rise and the difference in the optimised battery module were found to decrease by 36.48% and 44.36%, respectively. Cheng et al. [32] designed a finned forced air-cooled BTM, with aluminium herringbone fins connected to 18650 cylindrical LIBs. They concluded that the battery pack with fins reduced the maximum temperature rise of the battery by 17.63%. Li et al. [20] presented another ACS for LIBs with herringbone fins in a staggered cell layout and it reduced the average battery temperature by 4.15 °C at the discharging rate of 3C. Whereas Zhao et al. [33] used a cooling plate with a pin–fin to study the battery heat generation rate at a specific

Table 1
Thermal physical properties of battery [38,39].

Parameters	Value
Diameter	21 mm
Height	70 mm
Volume	2.42×10^{-5} m^3
Mass	66.67 g
Discharge Voltage	2.5 V
Nominal Capacity	4.6Ah
Nominal Voltage is	3.6 V
Density	2751 $kg.m^{-3}$
Specific heat capacity	1070 $J/(j.kg^{-1}\bullet K^{-1})$

discharge rate of 5C. The study concluded that the cooling plate with different size of pin-fins improves the battery's thermal performance. The results reported also showed that the fins significantly affect the cooling performance, allowing for the optimum battery temperature with the maximum temperature for batteries ranging between 15 °C and 35 °C. However, the fins were insufficient to maintain the temperature uniformity for a 5 °C temperature difference in the entire module volume. The distances between batteries and airflow direction were also decisive for a successful thermal design.

To summarise, as per the literature review above, the impacts of fins on the battery thermal performance have been studied by some researchers in some extend. However, most researchers used prismatic and pouch cells, which allowed them to attach the fins to the flat surface of a battery cell. Although fins can be used to enhance cooling in BTMS, there are still significant scientific knowledge gaps in understanding the efficiency of cooling fins in air-cooling cylindrical cells, which have a higher energy density than those types of cells [34]. By integrating the fins into the cylindrical cells, the system becomes overly compact due to the small size of the cells and the limited space of the battery back in EVs, making it extremely difficult to keep the battery back at the optimal operating temperature.

To address these knowledge gaps, in this paper a single cylindrical lithium battery module with cooling fins is designed and analysed using CFD simulation. The performances of the cell battery with ACS under different heat generation rates are investigated numerically. Both the transient internal and external temperatures for the battery are examined. The effects of the discharge rates and number, thickness, length, and rotation of the fins are investigated for the thermal performance of the cell based on the quantified heat generation rate of a commercial cell 21700 (NCM811). The effects of the loop of the spiral fins on heat dissipation are investigated, and the results are compared with the vertical fin's outcome. Since 21700 (NCM811) is a new generation of the battery and the published works on these cells are very limited, this study characterising the thermal performance of this specific LIB cell is crucial in the development and designing of a full-scale air-cooling BTMS.

This paper is divided into four sections, including the current section. Section 2 describes the model geometry and provides the details of the governing equations and numerical methods used to solve them, and in Section 3, the results are summarised and discussed in detail. Finally, conclusions of the study are provided in Section 4.

2. Geometry and numerical methods

2.1. Geometrical model

A $LiNi_{0.8}Co_{0.1}Mn_{0.1}O_2$ (NCM811) lithium-ion is regarded as one of the most competent positive electrode materials for LIBs [36]. The basic parameters of LIB 21700 type are considered and presented in Table 1. An air-cooled BTMS having Z-shape is one of the most used air-cooled BTMSs [37]. A 3D model of the battery and the geometry of LIBs with and without fins is shown in Fig. 1(a-d).

According to the literature survey, rectangular fins exhibit promising thermal performance in a variety of heat transfer applications [40]. Hence, the first part of the study is carried out using rectangular fins to investigate the effects of the fin number, rotation, thickness and length on the thermal performance of the module. The fins are attached to the 21700 Li-ion battery surface and extended into the surrounding air, with aluminium being chosen due to its low cost and lightweight [20], the thermal properties of aluminium and air are shown in Table 2. Secondly,

Table 2
Thermal properties of aluminium and air [41].

Material	Density (kg/m^3)	Specific Heat Capacity (J/kg K)	Thermal Conductivity (W/m K)	Viscosity ($kg/m\ s^{-1}$)
Air	1.16307	1006.4	0.0242	1.6036×10^{-5}
Aluminium		871	202.4	/

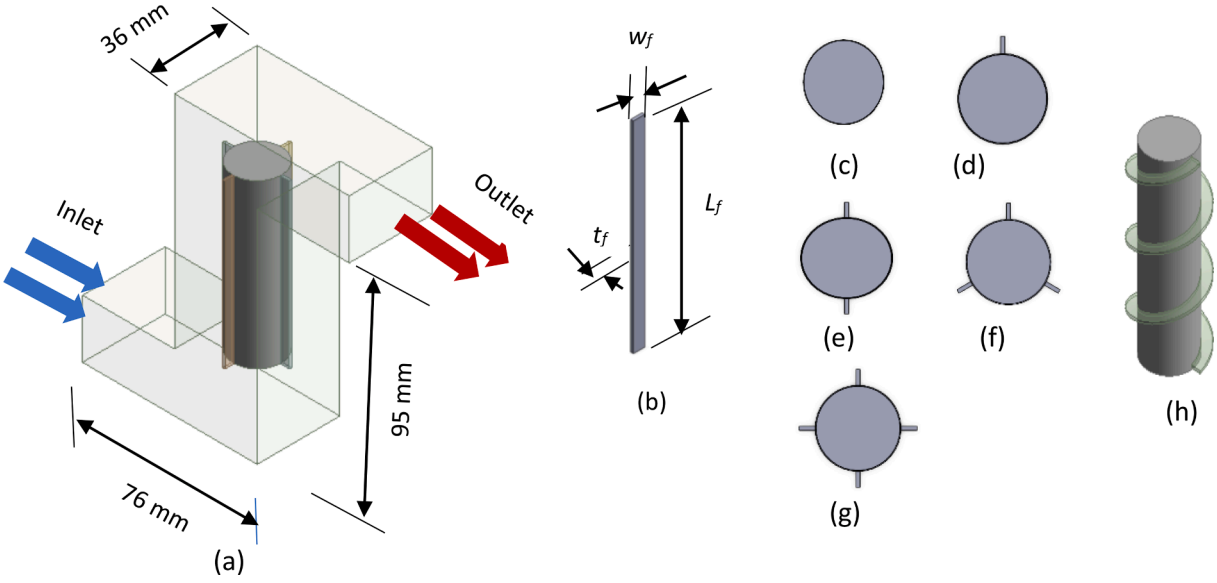

Fig. 1. (a) 3D model of a battery with vertical fins, (b) fin's dimensions, (c) top view of the cell without fins, (d) - (g) top view of the cell with 1, 2, 3 and 4 fins respectively, (h) 3D model of the battery with a spiral fin.

Table 3
Heat generation rate.

Discharge rate	$\varphi = A_0 + A_1 t + A_2 t^2 + A_3 t^3$				
	A_0	A_1	A_2	A_3	R^2
1.0C	0.1628	4×10^{-04}	-3×10^{-07}	9×10^{-11}	0.9959
1.5C	0.9988	1×10^{-05}	-1×10^{-07}	1×10^{-10}	0.9989
2.0C	2.0905	-6×10^{-4}	6×10^{-07}	7×10^{-11}	0.9978
2.5C	3.6299	9×10^{-4}	-2×10^{-06}	2×10^{-09}	0.9994

spiral fins with different loops will be applied around the battery, as shown in Fig. 1(h), and a comparison with the vertical fins will be reported.

2.2. Governing equations

The model is comprised of a cylindrical battery with internal heat generation and surrounding air; both the temperature and flow fields of the cell system should be calculated. Computational fluid dynamics (CFD) method is an effective way to calculate these fields. The governing equations are reported as follows [32–37].

Continuity equation

$$\frac{\partial u_i}{\partial x_i} = 0 \tag{1}$$

Momentum equation

$$\rho_{au_j}\frac{\partial u_i}{\partial x_j} = -\frac{\partial p}{\partial x_i} + \frac{\partial}{\partial x_j}\left[(\mu + \mu_t)\frac{\partial u_i}{\partial x_j}\right] \tag{2}$$

Turbulent kinetic energy (TKE) equation

$$\rho_a u_j \frac{\partial k}{\partial x_j} = \frac{\partial}{\partial x_j}\left[\left(\mu + \frac{\mu_t}{\sigma_k}\right)\frac{\partial k}{\partial x_j}\right] + \frac{\mu_t}{2}\left(\frac{\partial u_i}{\partial x_j} + \frac{\partial u_j}{\partial x_i}\right) - \rho_a \varepsilon \tag{3}$$

Turbulent kinetic energy dissipation rate equation

$$\rho_a u_j \frac{\partial \varepsilon}{\partial x_j} = \frac{\partial}{\partial x_j}\left[\left(\mu + \frac{\mu_t}{\sigma_k}\right)\frac{\partial \varepsilon}{\partial x_j}\right] + C_1 \frac{\mu_t}{2}\left(\frac{\partial u_i}{\partial x_j} + \frac{\partial u_j}{\partial x_i}\right)^2 \frac{\varepsilon}{k} - C_2 \rho_a \frac{\varepsilon^2}{k} \tag{4}$$

$$\text{Where } \mu_t = \rho C_\mu \frac{k^2}{\varepsilon} \tag{5}$$

Where u_i and u_j are the average velocity components, p is the average pressure. ρ_a, ε and k are the air density, the dissipation rate of the TKE, respectively. μ_t and μ are the turbulent dynamic viscosity and air's molecular dynamic viscosity coefficients, respectively.

Typical values of the parameters in the k-ε turbulence model are taken as $C_\mu = 0.09$; $C_1 = 1.44$; $C_2 = 1.92$; $\delta_k = 1.0$; $\delta_\varepsilon = 1.3$; $\delta_T = 0.85$ [42].

In the battery cell, as the heat generation rate changes with time, the transient temperature equations which can be used to obtain the temperature field of the system, are shown as below:

Energy transport equation for the airflow region

$$\rho_a C_{p,a}\frac{\partial T_a}{\partial_t} + \rho_a C_{p,a} u_j \frac{\partial T_a}{\partial x_j} = \frac{\partial}{\partial x_j}\left[\left(\lambda_a + \frac{\mu_t}{\sigma_T}\right)\frac{\partial T_a}{\partial x_j}\right] \tag{6}$$

The energy conservation equation of the battery is as follows.

$$\rho_b C_{p,b}\frac{\partial T_b}{\partial_t} = \frac{\partial}{\partial x_j}\left[\lambda_{b,j}\frac{\partial T_a}{\partial x_j}\right] + \varphi \tag{7}$$

Where T_b and T_a are the battery and air temperatures, respectively. λ_b and λ_a are the battery and air thermal conductivity, respectively. $C_{p,a}$ is the air heat capacity and φ is the battery heat generation rate.

The battery heat generation rate, which was experimentally determined by Sheng et al. [39] as a function of the state of charge (SOC), is expressed as a function of time as required in the simulation. Therefore, galvanostatic discharge is applied so that the SOC varies linearly as a function of time. Then, the equivalent equation of heat generation as a function of time is obtained and integrated into the ANSYS Fluent solver to calculate the battery temperature during the discharge process. Four different discharge rates (i.e. current rates) at 1C, 1.5C, 2C and 2.5C were applied, respectively. Their contribution to the heat generation rate is shown in Table 3, where A is the equation coefficient, and t is the discharge time of the cell.

2.3. Boundary conditions

The following boundary conditions were set for the battery model to achieve an accurate solution.

- Initial inlet air and battery temperature were set to be all 30 °C, and the ambient pressure was assumed to be standard atmospheric pressure.
- Air inlet: velocity inlet; air outlet: a pressure outlet with a gauge pressure of 0 Pa.
- Non-slip and adiabatic conditions are imposed on the surrounding walls of the system.
- Fluid-solid interface: the contact surface between the battery surface and air was set as a fluid–solid coupling boundary.
- The convective heat transfer coefficient between battery and air is written as follows [43]:

$$\mathrm{h} = 0.0374\left(k_f / D_h\right) R_e^{0.8014} \tag{8}$$

$$R_e = \rho_a V D_h / \mu_a \tag{9}$$

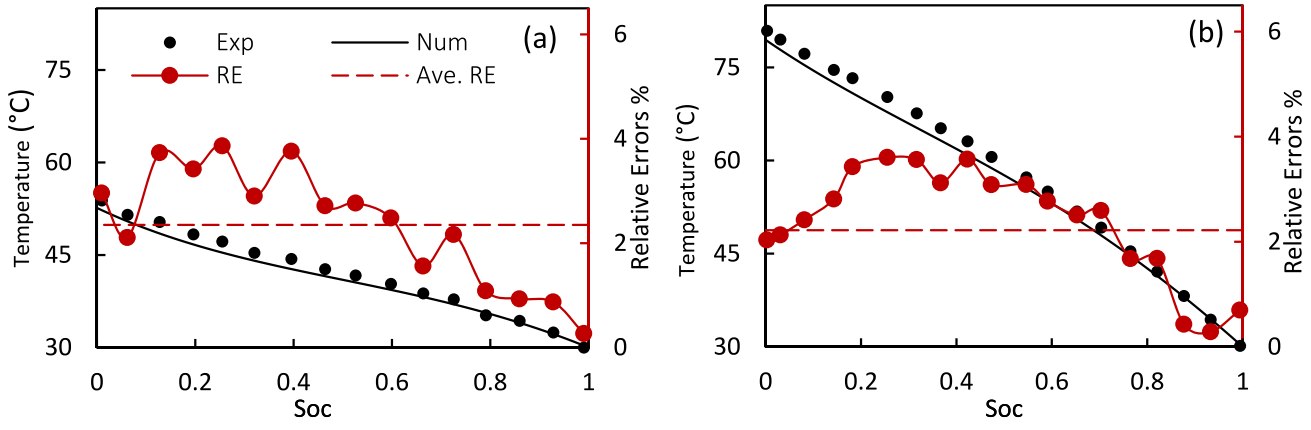

Fig. 2. Cell temperature comparison between simulation and experiment at different discharge rates: (a) 1.5C and (b) 2.5C.

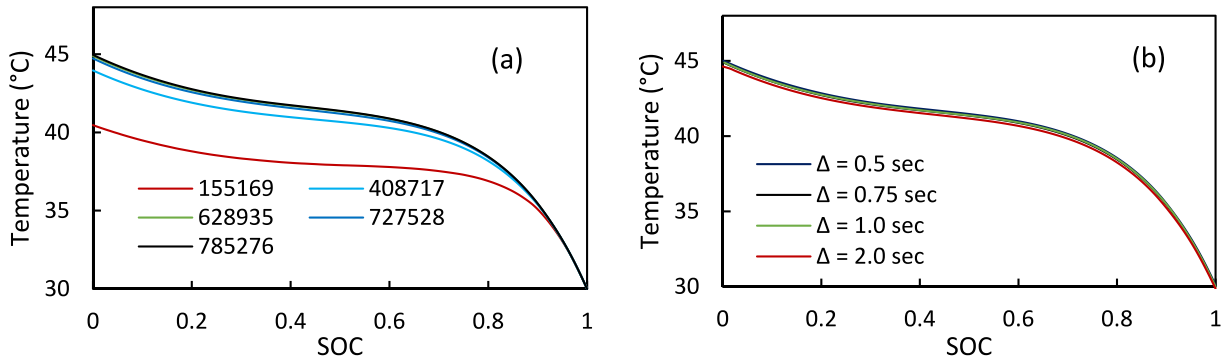

Fig. 3. (a) Grid independence test, (b) time step independence test.

Where k_f and μ_a are the thermal conductivity and the dynamic viscosity of air, respectively, and D_h is the hydraulic diameter of the duct.

2.4. Numerical methods

The commercial CFD programme ANSYS 2021R1 Fluent was used to perform the 3D numerical simulation in this work. Before this stage, SolidWorks software was used to create the physical models. The finite volume method in ANSYS used to discretise the governing equations with a second-order upwind scheme to solve the discretised equations, where the unknown quantities at the cell faces are computed by using a multidimensional linear reconstruction approach described in [44] to achieve even higher order at the cell faces through a Taylor series expansion of the cell centred solution about the cell centroid. The SIMPLE algorithm of Patankar [45] was then chosen to solve the pressure-based equation derived from the momentum and mass continuity equations so that the velocity and pressure fields are coupled to each other and solved by adopting an iterative solution strategy. All these equations were solved sequentially and iteratively, and the relaxation factors for the pressure correction, density, momentum, and thermal energy were used as 0.3, 1, 0.7 and 1, respectively.

2.5. Model verification

To validate the numerical prediction of the battery cell heat generation rate, a comparison is made with the experiment data of Sheng et al. [31], where the experimental testing was carried out under free convection conditions at the battery cell discharge of 1.5C and 2.5C with a constant current. The surrounding temperature was kept at 30 °C during the test. A comparison of the maximum battery temperature between the experimental and simulated results is presented in Fig. 2. As seen, the simulation agrees well with the experimental data, as the maximum relative error and its average were recorded as 3.8% and 2.3%, respectively. The average Relative Errors (RE) of the cell temperature between the experimental and numerical data can be defined in Eq. (10) as:

$$RE = \frac{1}{N}\sum \frac{|T_{exp} - T_{num}|}{T_{exp}} \times 100 \tag{10}$$

In general, the relative error between the simulated value and the experimental data was within 2.66%, which further demonstrates that the computational method for the heat generation rate of the cell battery is accurate.

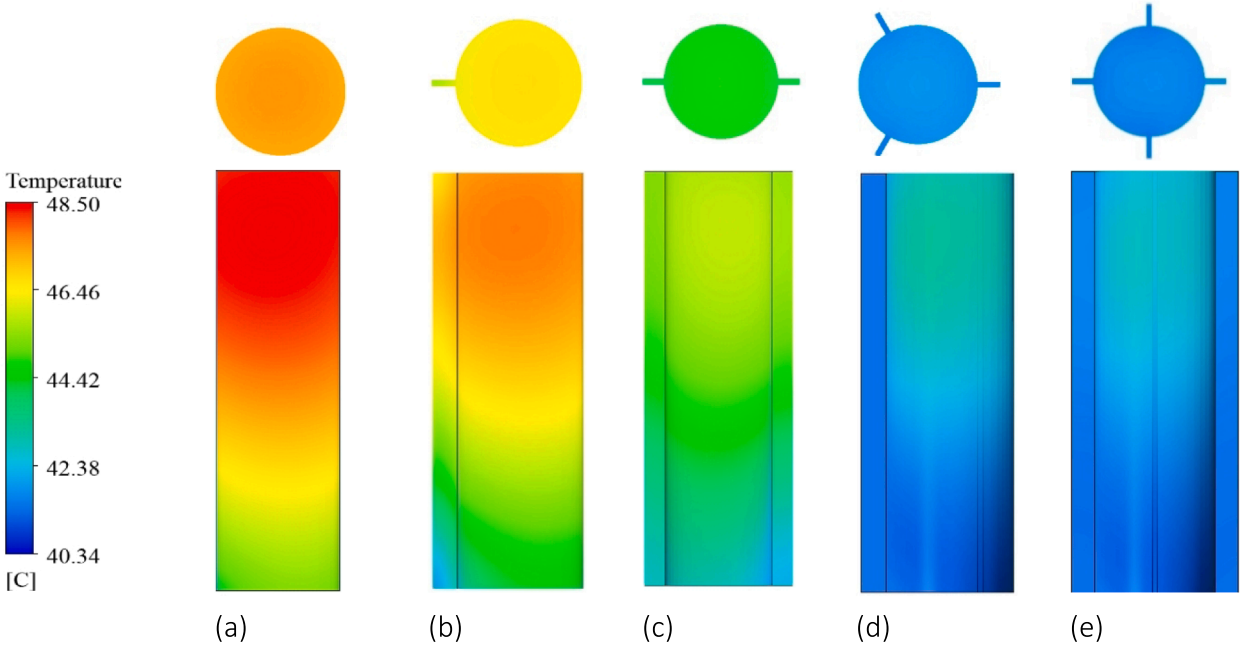

Fig. 4. Contours of temperature distribution in the XY and XZ planes at 2.5C, $Re = 7515$ with different fins numbers where (a) no fin; (b) 1 fin; (c) 2 fins; (d) 3 fins; and (d) 4 fins.

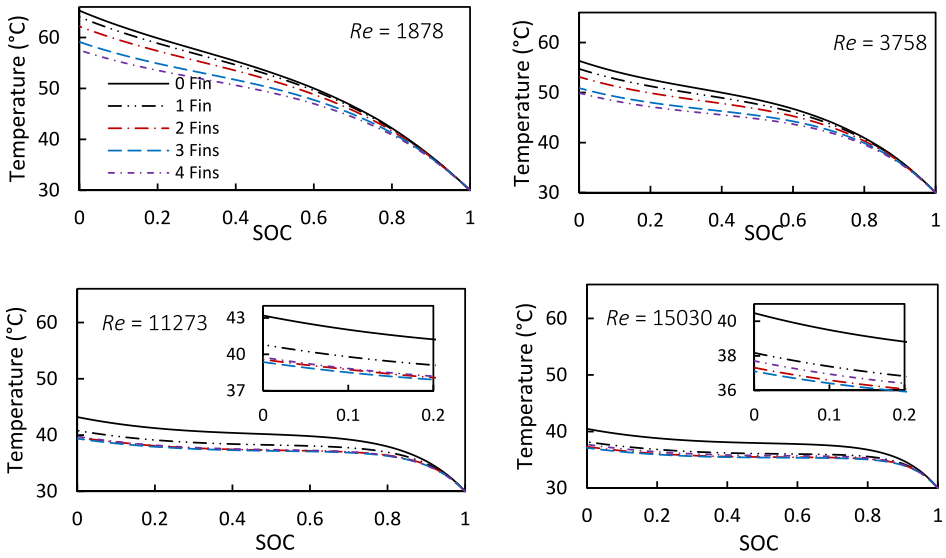

Fig. 5. Cell temperature distribution at discharge rate 2.5C with different Reynolds numbers.

Table 4
Drop in Cell Temperature.

Re	$T_{b,0fins}$	$T_{b,4fins}$	The drop in Cell Temperature		
			Total drop $T_{b,0Fins}$ -$T_{b,4fins}$	By Forced *80* - $T_{b,0fins}$	By Fins *80* - $T_{b,0fins}$
1878	65.3	57.5	22.5	14.7 (65%)	7.8 (35%)
3758	56.3	49.9	30.1	23.7 (80%)	6.4 (20%)
7515	47.8	43	37	32.2 (89%)	4.8 (11%)
11273	43.2	39	41	36.8 (92%)	4.2 (8%)
15030	40.5	37.7	42.3	39.5 (93%)	2.8 (7%)

2.6. Grid and time-step independence tests

To examine and ensure that the numerical results are independent to the grid and timestep used, the cell temperature obtained by the four different grid numbers against the SOC is reported in Fig. 3(a). In this case, the discharge rate with 2 vertical fins is 2.5C, and Re = 7515, Ta = 30 °C and Δt = 0.5 s. The variation in the grid number has a little impact on the temperature rise when the number of nodes ≥628935. Moreover, the temperature variation among the mesh nodes 628935, 727528 and 785276 is only around 0.4% and 0.35%, respectively, so 727528 mesh was chosen to conduct the further simulations. To assess the time step in the numerical simulation, the cell temperature is presented in Fig. 3(b) at the discharge rate of 2.5C and 727528 mesh, with different time step sizes of 0.5 s, 0.75 s, 1 s and 2 s. As can be seen, there is not much difference in the results with the chosen time steps, and the discrepancy between the temperatures for the time steps of 0.5 s and 2 s was within 0.82%. Therefore, a time step size of 1 s is being considered to minimise the total simulation time while also to maintain the numerical stability.

3. Results and discussion

3.1. Effects of vertical fins and Reynolds number on the cell temperature

Fig. 4 shows the temperature distributions at the symmetrical plane as well as the middle cross-section of the battery at the end of discharge rate of 2.5C using the different fin numbers. As can be seen, when it is compared to the inner section, the heat dissipation rate from the cell surface to the air is extremely high, and a heat build-up occurs at the battery core. So, the middle part of the cylindrical cell had the highest temperature, while the outer surface had the lowest.

The performance of the different fin structure layouts is analysed and compared using the battery cell temperature at 2.5C discharge rates at the four different Reynolds numbers as in Fig. 5. As the Reynolds number increases, there appears to be a significant temperature decrease due to flow turbulence and enhanced heat transfer, resulting in the increased rate of heat absorption by air. Experimentally, under the free convection condition, the battery temperature reached 80 °C at 2.5C [36], and this result is used to evaluate the current numerical results, as reported in Table 4. By increasing Re from 1875 to 15030, the forced convection effect on the temperature drop increases from 65% to 93%, while the effect of fins decreases from 35% to 7%. These results therefore indicate that under the simulation conditions, the fins become more effective at a low Re.

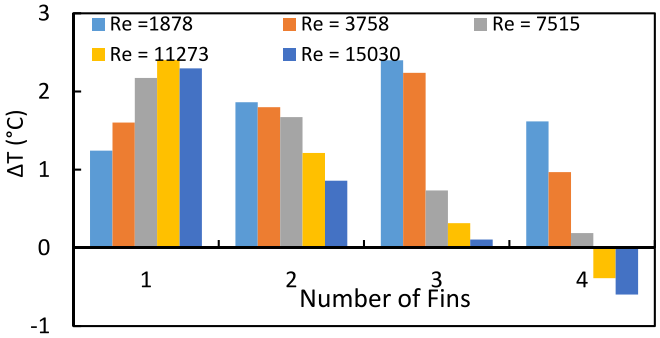

Fig. 6. The temperature divergence between the fins at different Reynolds numbers and 2.5C.

Moreover, the fin numbers are significant when calculating the thermal performance and associated costs. Fig. 6 shows the temperature differences between the cells at various fins number obtained by Eq. (11)

$$\Delta T_{b,j} = \left(T_{b,j} - T_{b,j+1}\right), \tag{11}$$

where j is the number of fins (0, 1, 2 and 3).

The results indicated that applying fins to the outer surface of the battery can significantly increase the convection heat transfer, but the number of fins affect its, that is a high Re with 3 fins provides a better cell cooling rate compared to 4 fins. At Re = 11273 and 15030, the cell temperature with 3 fins is 39.36 °C and 37 °C, respectively while for 4 fins it is 39.75 °C, 37.7 °C.

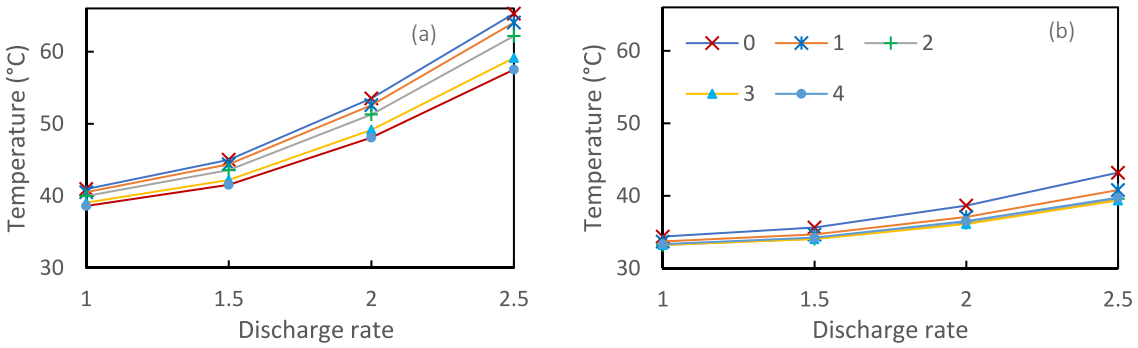

Fig. 7. Effect of the discharge rate on the battery temperatures at (a) *Re* = 1878 and (b) *Re* = 11273.

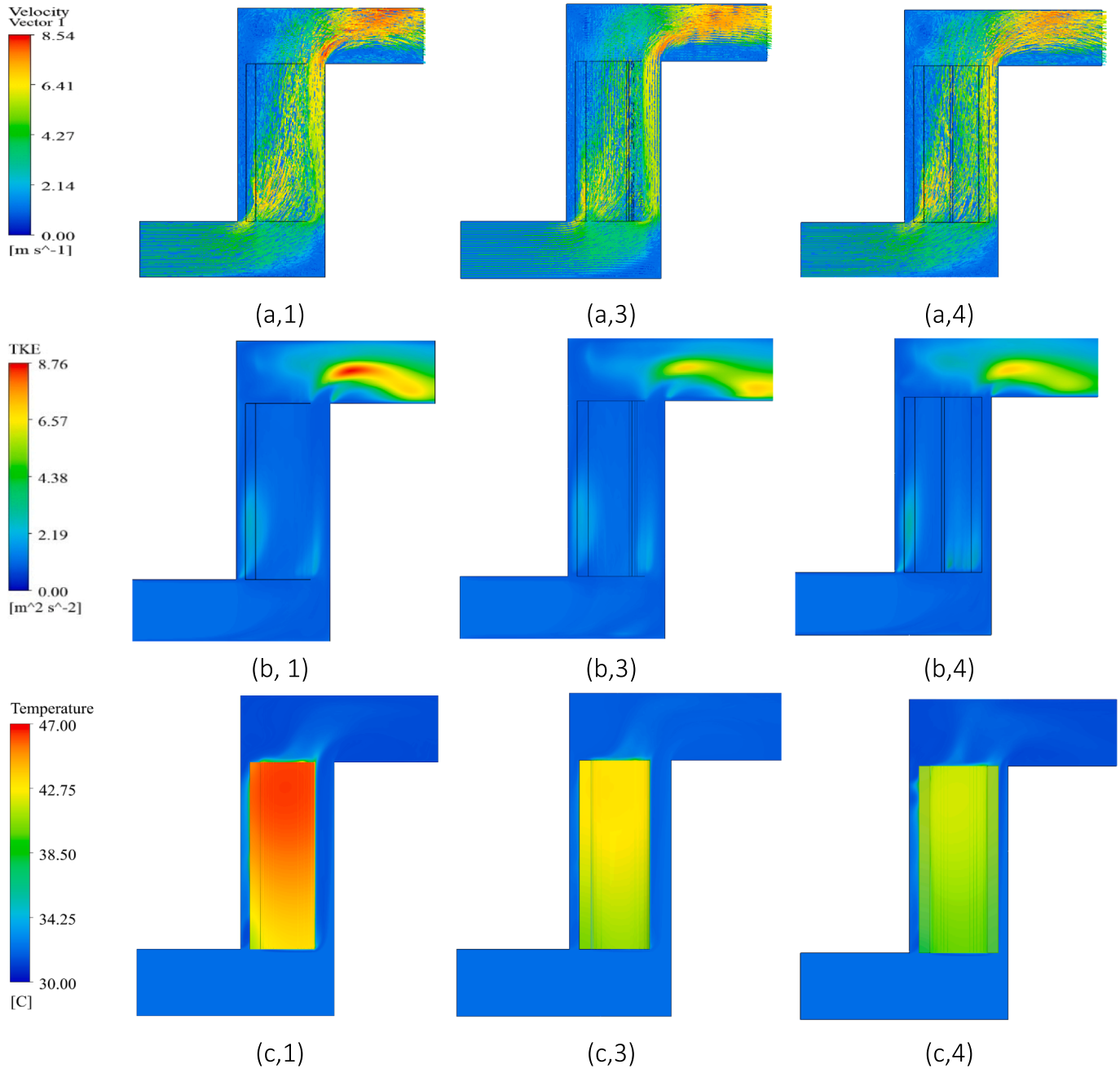

Fig. 8. Contours of velocity (a) and TKE (b) distributions in the XY at 2.5C, *Re* = 7515 with different fins numbers where 1, 3 and 4 indicate the number of fins, respectively.

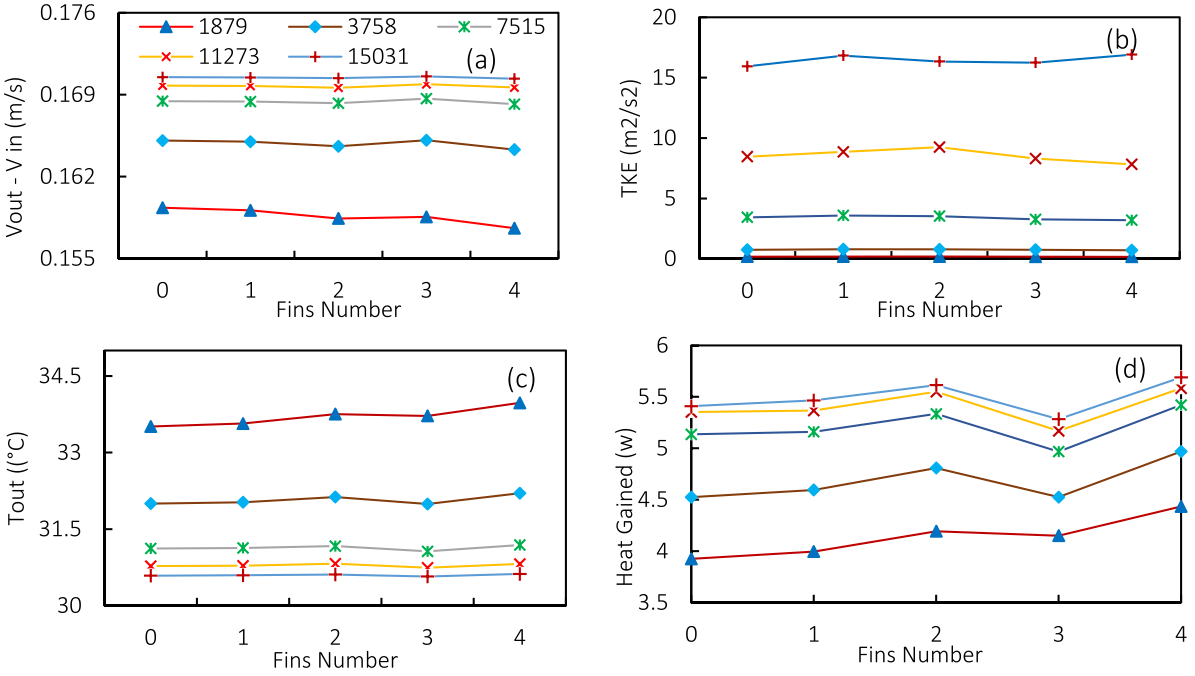

Fig. 9. Outlet air parameters at 2.5C where (a) outlet velocity, (b) TKE, (c) outlet temperature and (d) heat gained.

3.2. Effect of discharge rate

The battery temperatures under different discharge rates from 1C, 1.5C, 2C and 2.5C are simulated with different numbers of vertical fin. Here, the results with $Re = 1878$ in Fig. 7(a) and 11273 in Fig. 7(b) are shown as an example for this analysis. The results generally showed that the battery temperature at the final discharge rate increased as the rate change increased. However, the temperature increase become less as the Reynolds number becomes higher; for example, for $Re = 1878$ and 4 fins with an increase in the discharge rate from 1C to 2.5C, the temperature is increased by 32.88% (38.6 °C–57.51 °C), while that at $Re = 11273$ is increased about 16.3% (33.3–39.7). With an increasing Reynolds number, the battery temperature-rise curves move downward, which indicates that the effectiveness of the air cooling is gradually enhanced the heat transfer rate.

3.3. Roles of flow physics and thermal transport

Fig. 8 provides the contours of the velocity, TKE and temperature. These results show that the cooling air is rapidly accelerated into the cell from the left side of the duct, creating a local high entrance velocity as a result of the high heat transfer from the battery surfaces, as in Fig. 8(a). With an increase in the number of fins, there is a slight drop in the velocity magnitude which is related to the fin constraining the airflow, thus impacting on the velocity reduced by 3.5% and the TKE by 19%. It can be further seen from Fig. 8(b,4) that the flow turbulence started to intensify around the cell, and a high of turbulence and mixing near the cells caused a more significant amount of fresh air to transport heat away from the cells, which further led to the reduction in the battery temperature in this location. On the other hand, the TKE reached its maximum value above the cell where the air changed its flow direction to the outlet. Finally, as shown in Fig. 8(c), the cell temperature increases from the bottom to the top of the cell because of the air temperature increase and less amount of low-temperature air is available to take the heat away from the cells, where the thermal field of air is more apparent at both the side and top of the cell.

3.3.1. Outlet air parameters

Different thermal parameters of air outlet, velocity, TKE and temperature, are shown in Fig. 9(a-b). As seen in Fig. 9(a), with an increase in the Reynolds number, the velocity profile is enhanced, but the rate of increase becomes less at a high Re. For instance, the velocity for 2 fins is increased by 3.7% (0.158 to 0.264 m/s) when Re is increased from 1879 to 3758, while, it is only 0.47% (0.169 to 0.171 m/s) when Re is changed from 11273 to 15031. Also, the same behaviour can be noticed for TKE in Fig. 9(b). The TKE increases by 76.5% (0.184 to 0.783 m^2/s^2) when Re increases from 1879 to 3758, but by 43.4% (9.244 to 16.34 m^2/s^2) as Re increases from 11273 to 15031. These variations in the velocity and TKE profiles can also be reflected on the temperature profile, as with an increase in the air outlet velocity, it is expected that the battery temperature would be dropped as a result of more heat being removed from the system; and consequently, this leads to a reduction in the temperature of air outlet as can be seen in Fig. 9(c).

Moreover, at a low $Re = 1879$, with an increase in the fin number from 0 to 4, there is an evident change in the velocity and temperature profiles, while for a high $Re = 15031$, both the profiles are nearly remain constant, which indicates that there is no significant change in the battery temperature, proving further evidence on the early results where the fin number became less effective at a high Reynolds number. However, at a high Reynolds number, the cell with 3 fins produces the highest outlet velocity compared to 2 fins and 4 fins, so the airflow turbulence in the model cell with 3 fins is deemed to be optimal, where the fin location around the cell does not inhibit the airflow.

The aluminium battery case is assumed to have a low emissivity and is in good insulation. So, both the radiation and heat loss from the module were disregarded. Therefore, the heat transfer from the cells absorbed by cooling air through the air temperature rise can be calculated by

$$Q_T = \dot{m} C_p (T_{out} - T_{in}) \tag{12}$$

The mass flow rate of air cooling $\dot{m}$ can be calculated from

$$\dot{m} = \rho A_{duct} V \tag{13}$$

where, A_{duct} is the duct area, and T_{out}, T_{in}, C_p, ρ and V are the air outlet, inlet, specific heat capacity, density, and velocity, respectively.

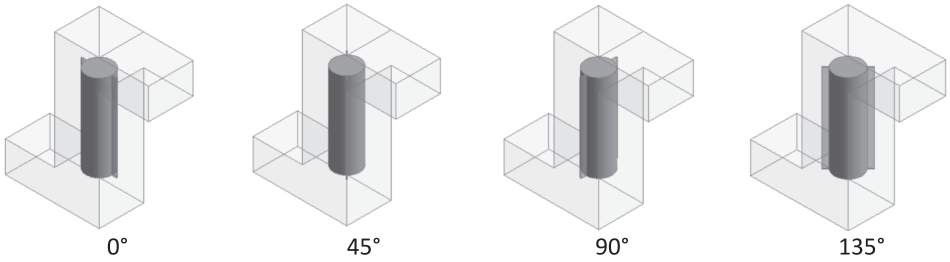

Fig. 10. Rotation of the battery with 2 fins.

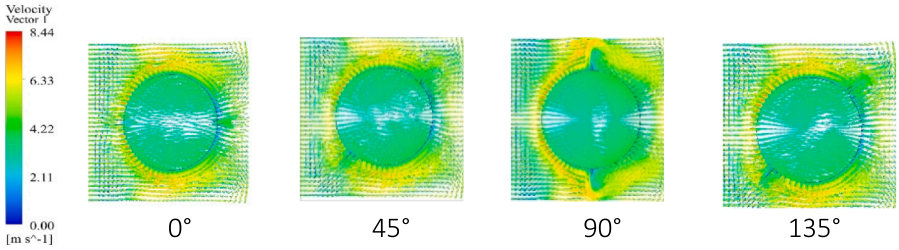

Fig. 11. Velocity vectors around the model of a battery with 2 fins.

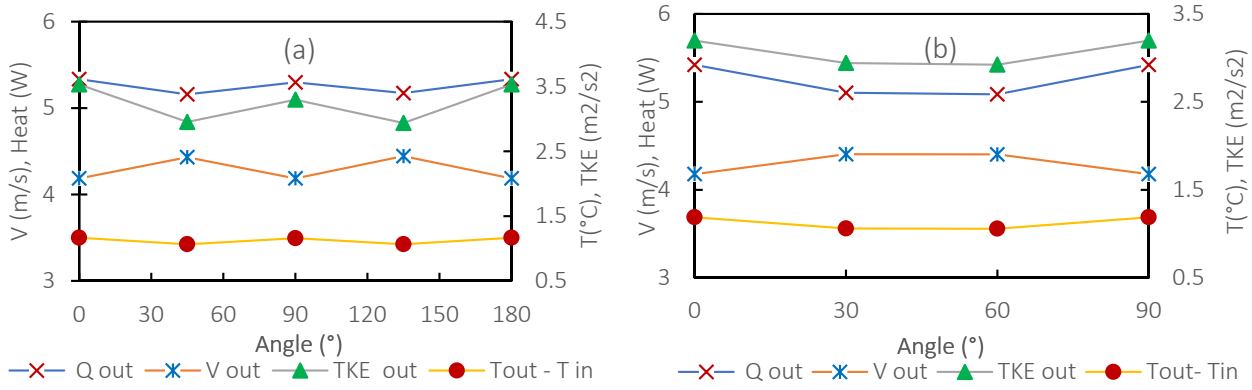

Fig. 12. Effect of fin's rotation on the air outlet parameters where (a) 2 fins, (b) 4 fins and $Re = 7515$.

Fig. 9 (c) provided the heat gain as it is evident with the increase in both *Re* and number of fins, heat gained increased, and there is a drop in value at the 3 fins case, which becomes more apparent when $Re \geq 3758$ and where more cooling occurs to the battery temperature.

3.4. *Effect of fin rotation*

In this part of the investigation, we report the effect of the rotation of the fins on the air-cooling performance considering 2 and 4 fins. As can be seen in Fig. 10, when changing the battery angle from 0° to 135°, the location of the fins will also be changed. The focus here is to investigate the potential impacts on battery cooling.

Fig. 11 presents the velocity vectors around the battery cell with different fin angles in the mid horizontal cross-section zone. As can be seen, the flow region around the cell is changed as the fin's angle is changed to different positions. At the angle of 0° the velocity is mostly

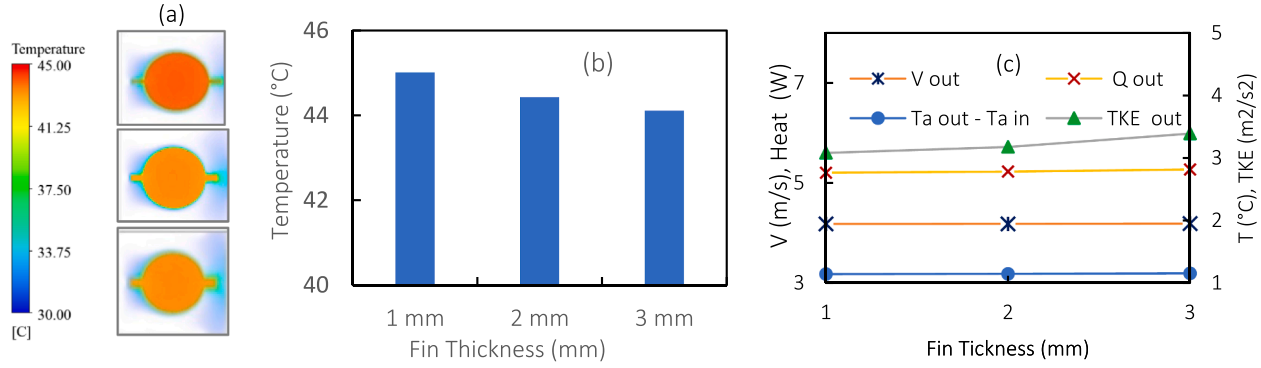

Fig. 13. Effect of the fin's thickness on (a) thermal filed; (b) cell temperature; (c) outlet air thermal parameters at 2.5C and $Re = 7515$.

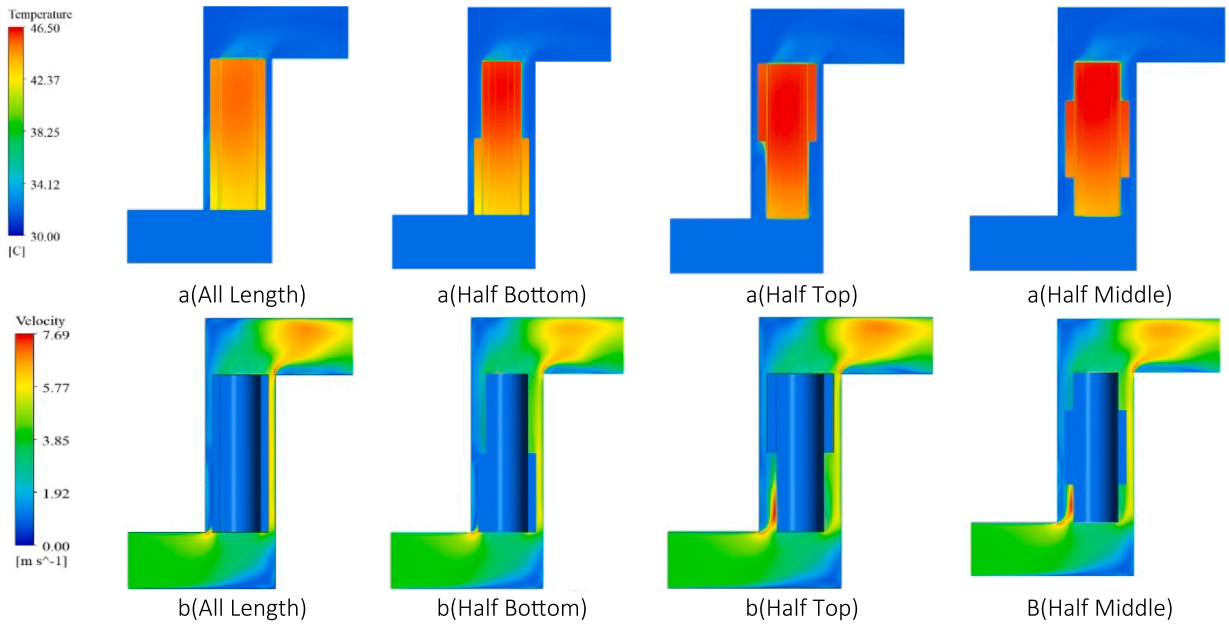

Fig. 14. Contours of (a) thermal field; (b) air velocity.

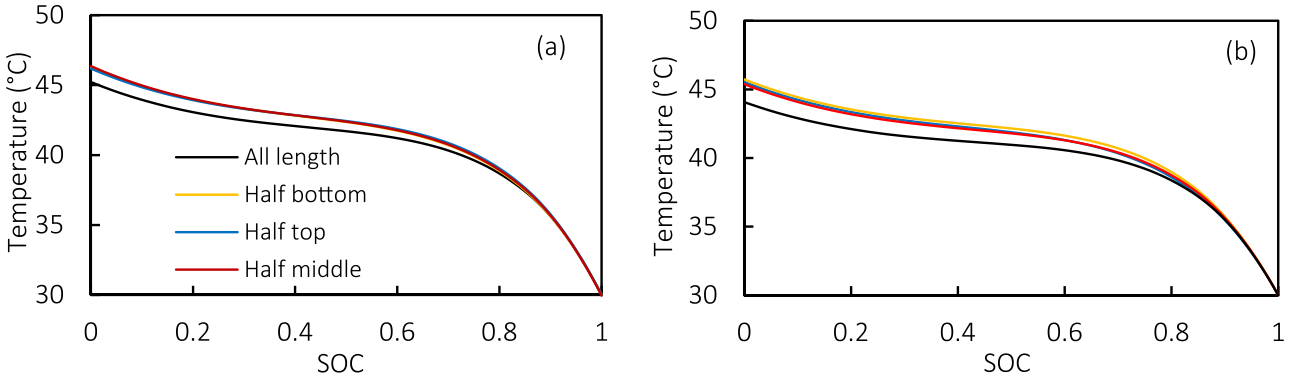

Fig. 15. Battery temperature with different fin lengths and locations where (a) 2 fins and (b) 3 fins.

reached its maximum very close to the cell, which increases the heat transfer rate between the air and cell, leading to a reduced cell temperature to 45 °C. However, in the 134° case, the fins become a barrier to the flow around the cell, especially in the area located after the fins, so their effect on air cooling is reduced and as a consequent, the cell temperature reaches 46.3 °C.

Additional thermal parameters of the air outlet are reported in Fig. 12(a). While the maximum and minimum battery temperature for 4 fins are 42.28 °C at 60° and 42.11 °C at 0°, respectively. It should also be noted that at 180° and 90° in Fig. 12(b), the cell returns to its initial position, and that the fins generally become more effective in cooling for both cases when the battery is placed at 0°, where the heat transfer by air reaches its maximum value, as shown in Fig. 12(b).

3.5. Effect of Fin's thickness and length

The fin's thickness and its length influence both the mass of heat dissipation around the cell and the manufacturing cost, so this section presents a numerical investigation of the fin's thickness and length on the thermal performance of cell cooling. From Fig. 13, it can be observed that an increase in the fin's thickness enhanced the heat dissipation from the cell; however, from 1 mm to 3 mm, the temperature is dropped by 2%, Fig. 13(b). The reason for is that the heat conduction is increased between the cell and fins, as the contact between the cell surface and fresh air becomes less. This result agrees with the previous funding [46]. For the air outlet thermal parameters, there is no significant change observed except for TKE, and TKE increases with the thickness of fins due to the increase in inhibiting the airflow.

The temperature and velocity contours at the different fins length and locations are depicted in Fig. 14, where the size of the fins is reduced to half and located in the bottom, top and middle of the cell surface and compared with the results of the dynamic behaviour of a cell having a full fin at 2.5C and $Re = 7515$ shown in Fig. 15. The lowest cell temperature is recorded when all the fins are applied around the cell as 45 °C and 44.1 °C for 2 and 3 fins respectively. When using the half fins, the cell temperature increases by less than 2.5% and 3% for 2 and 3 fins, respectively. Moreover, the results in Fig. 15 show that the location of the half fins has no significant effect on the cell temperature, with only a 0.2 °C difference between the maximum and minimum temperature for the top, middle and bottom locations for 2 and 3 fins.

3.6. Analysis of spiral fin

3.6.1. Effects of number of loops on the cell temperature

Turbulence in the fluid flow influenced the convection heat transfer coefficient, so to further investigate this, spiral fins were mounted on the

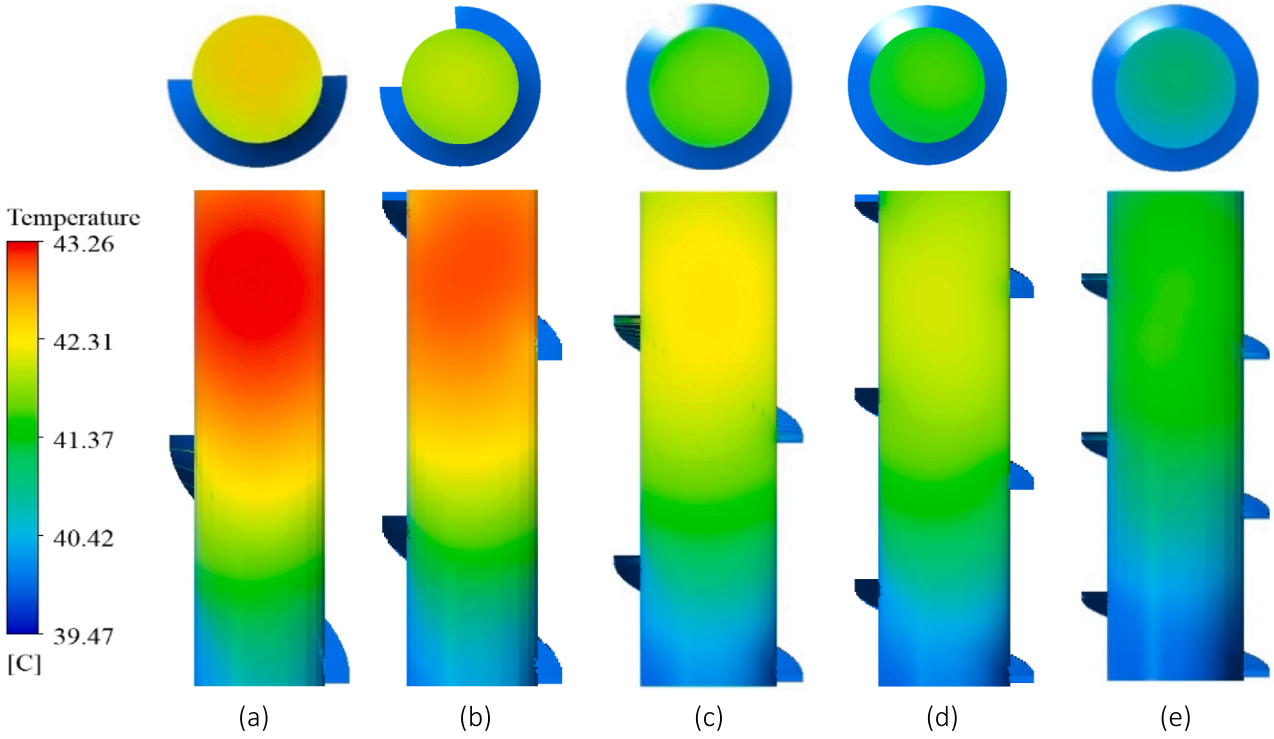

Fig. 16. Contours of temperature distribution in the XY and XZ planes at 2.5C, *Re* = 7515 with different spiral fins where (a) 1 loop; (b) 1.5 loops; (c) 2 loops; (c) 2.5 loops and (e) 3 loops.

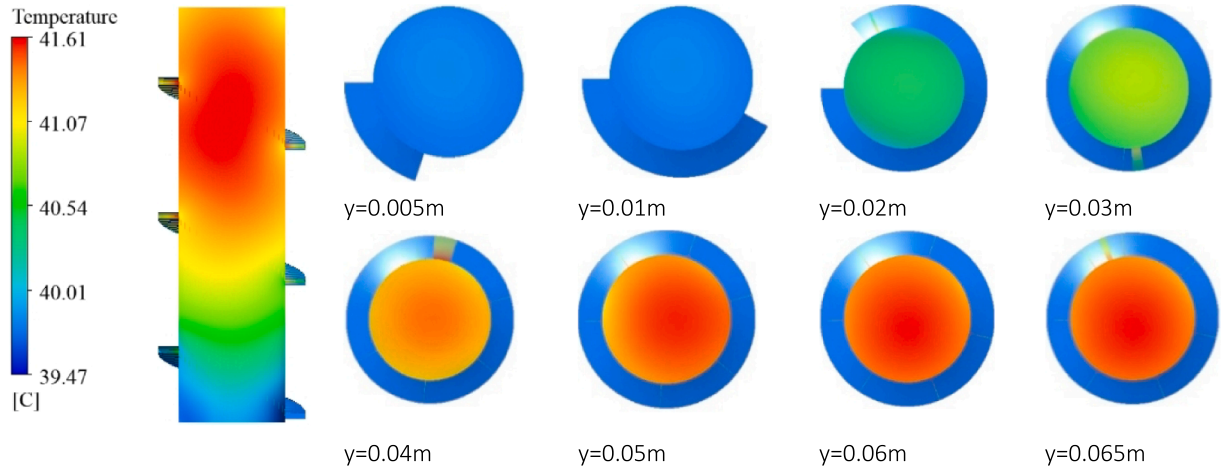

Fig. 17. Contours of temperature distribution in the XZ plane at different vertical positions with 7 mm fin pitch and a discharge rate of 2.5C.

outer surface of the battery cell. Fin loops 1, 1.5, 2, 2.5 and 3, correspond to the respective fin pitches of 21 mm, 14 mm, 10.5 mm, 8.5 mm, and 7 mm. In all the cases, the thickness and width of the fin were kept as 1 mm and 4 mm respectively. The temperature contours of the cell and fins can be observed in Fig. 16 as the battery temperature gradually increases from the bottom to the top of the battery due to convection. The results in Fig. 17 show that the temperature gradually decreases in the radial direction and is affected by the spiral fin along the cell.

The results of cell temperature at the end of the discharge rate 2.5C for *Re* = 7515 are shown in Fig. 18(a), further revealing that the cell temperatures are lower when the spiral fin is introduced. Interestingly, when the loop is increased, the cell temperature is reduced by 10.8 %, 12.6%, and 14.22% for the fin loops of 1, 2, and 3, respectively as compared to the finless cell. The temperature for the cell with 1 loop and 3 loops is 43.2 °C and 41.6 °C respectively.

3.6.2. *Outlet air parameters*

Fig. 19 shows the contours of air velocity and TKE with different fin loops. As seen again that the addition of spiral fins to the outer surface of the cell battery significantly enhances the heat transfer rate between the cell and cooled air. The configuration of the fin loops affects the rate of heat transfer. Moreover, turbulent flow is evident around the fins as demonstrated by the TKE.

The results in Fig. 18 (b) revealed that, comparing with a 1 fin loop, the velocity of the outlet air is relatively increased by 0.32%, 0.66% and 0.9% for those with fin loops of 1.5, 2, and 3, respectively, while for the TKE it increases by 4.9%, 6.7% and 10.5%, respectively. The air takes in sharp turn around the cell, and the fluid undergoes irregular fluctuations intensifying mixing, and there is a substantial breaking away of the fluid from the fins and cell wall – all of which are favourable to increased cooling of the cell.

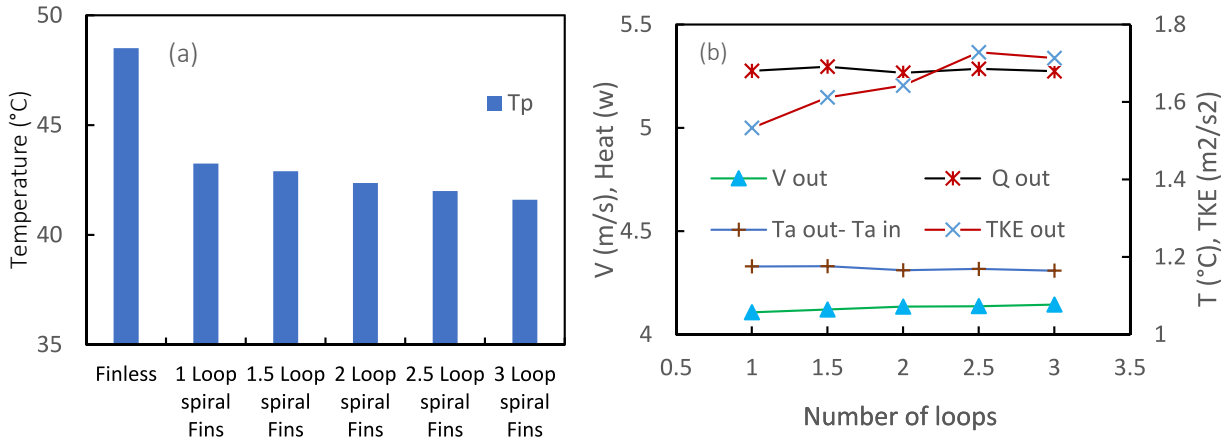

Fig. 18. Battery temperature at different loops of spiral fins.

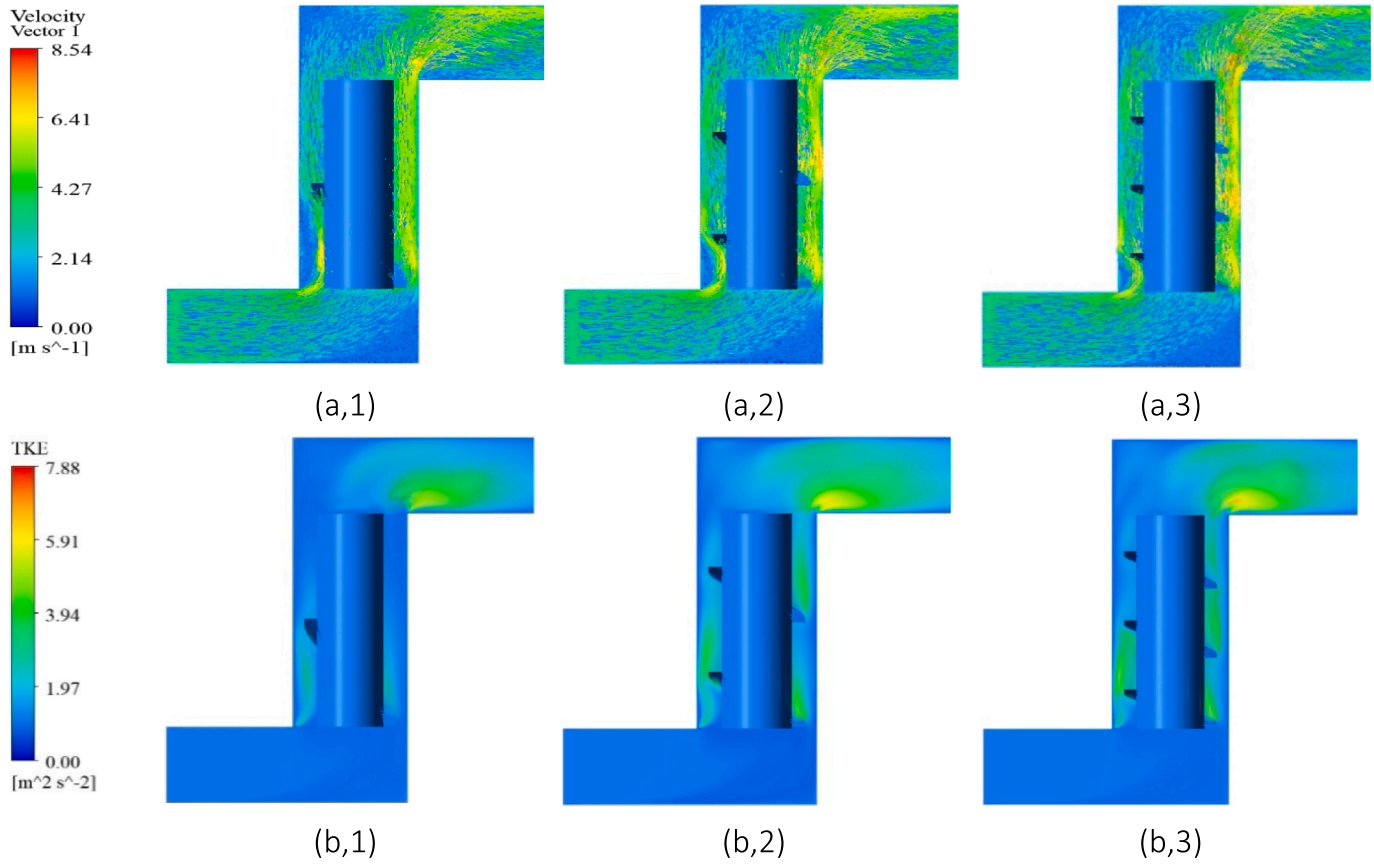

Fig. 19. Contours of (a) velocity and (b) TKE with different fin loops.

Overall, when comparing the thermal performance of vertical and spiral fins, the vertical 4 fins along the cell at $Re = 7515$ result in a cell temperature of 43 °C; whereas the spiral fins with 1, 2, and 3 loops result in cell temperature drop, respectively 43.2 °C at 0.46%, 42.36 °C at 1.5%, and 41.6 °C at 3.2%. So, as can be seen, approximately the cell temperature of a cell with 4 fins is equal to that of a cell with the spiral fins of 1 loop (43 °C ≈ 43.2 °C) when the fins have the same width and thickness. In the case of 4 vertical fins, by using the spiral fins with 1, 2 and 3 loops, therefore, save around 65.6%, 46.7% and 25% of the fin's material. These results further indicate that the spiral fins have several other advantages, such as a high heat transfer rate and a lower production cost.

4. Conclusions

This work investigated the dynamic behaviour of Lithium-ion battery temperature using air cooling. It revealed that the longitudinal fins around the cylindrical batteries favourably influenced the heat transfer generated in the battery. A series of numerical simulations were run to investigate the impacts of the fin's rotation, thickness, length, number, and position at various current rates. The extensive research of these aspects allowed for a more accurate perception when constructing a thermal management system of battery with cooling fins and air cooling. The main conclusions of this work are as follows.

- The reduction in the battery temperature was affected mainly by the Reynolds number, and the influence of fins became more effective at a low Reynolds number. In terms of the vertical fin number, it is often understood that increasing the fin number around the cell will enhance the heat transfer, but the results indicated that at a high Reynolds number 15030, the cell temperature with 3 and 4 fins was 37 °C and 37.7 °C respectively, which showed increasing the number of fins inhibited the airflow around the cell.
- The cell temperature was found to decrease but the heat transfer enhanced further when the fin's thickness was increased; however, with the compromise of the fin length to its half, in the 3 fins case, the maximum increase in the cell temperature was 1.5 °C, which was obtained when the fins located at the bottom of the cell. Related to the locations of the half fins (i.e., top, middle and bottom), the results indicated that these changes did not impact the overall solutions much.
- The vertical fin's orientation affected the heat exchange between the cell and cooling air. The cell temperature obtained was relatively low when one of the fins was positioned parallel to the inlet airflow direction.
- Adding a spiral fin to the outside surface of the battery cell significantly improved the heat transfer performance in the cell model, which reduced the cell temperature by 3.2% and the material usage by 25% to 65.6%. Therefore, spiral fins for thermal management systems in lithium batteries are potentially a promising option.

Declaration of Competing Interest

The authors declare that they have no known competing financial interests or personal relationships that could have appeared to influence the work reported in this paper.

Data availability

Data will be made available on request.

Acknowledgement

This work was supported by the University of Glasgow and Ali Alzwayi currently holds a Daphne Jackson Trust Fellowship (Ref: 401/003) funded by the Engineering and Physical Sciences Research Council (EPSRC).

References

[1] G. Zhao, X. Wang, M. Negnevitsky, H. Zhang, A review of air-cooling battery thermal management systems for electric and hybrid electric vehicles, J. Power Sources 501 (2021).
[2] I.B. Mansir, N. Sinaga, N. Farouk, U.F. Alqsair, C. Diyoke, D.D. Nguyen, Assessment of the effect of distance between lithium-ion batteries with a number of triangular blades, on the thermal management of the battery pack in a chamber full of phase change material, J. Storage Mater. 51 (2022), 104391.
[3] R. Youssef, M.S. Hosen, J. He, J. Jaguemont, M. Akbarzadeh, L. De Sutter, J. Van Mierlo, M. Berecibar, Experimental and numerical study on the thermal behavior of a large lithium-ion prismatic cell with natural air convection, IEEE Trans. Ind. Appl. 57 (6) (2021) 6475–6482.
[4] S. Wilke, B. Schweitzer, S. Khateeb, S. Al-Hallaj, Preventing thermal runaway propagation in lithium ion battery packs using a phase change composite material: An experimental study, J. Power Sources 340 (2017) 51–59.
[5] A. Väyrynen, J. Salminen, Lithium ion battery production, J. Chem. Thermodyn. 46 (2012) 80–85.
[6] L. Saw, Y. Ye, A. Tay, Electro-thermal analysis and integration issues of lithium ion battery for electric vehicles, Appl. Energy 131 (2014) 97–107.
[7] Z. Rao, Y. Huo, X. Liu, G. Zhang, Experimental investigation of battery thermal management system for electric vehicle based on paraffin/copper foam, J. Energy Inst. 88 (3) (2015) 241–246.
[8] M. Luo, J. Cao, N. Liu, Z. Zhang, X. Fang, Experimental and simulative investigations on a water immersion cooling system for cylindrical battery cells, Front. Energy Res. 10 (2022).
[9] M. Öztop, A. Şahinaslan, Control of temperature distribution for Li-ion battery modules via longitudinal fins, J. Storage Mater. 52 (2022), 104760.
[10] Q. Gao, G. Wang, Y. Yan, Y. Wang, Thermal management optimization of a lithium-ion battery module with graphite sheet fins and liquid cold plates, Autom. Innov. 3 (4) (2020) 336–346.
[11] H. Behi, D. Karimi, J. Jaguemont, F. Gandoman, T. Kalogiannis, M. Berecibar, J. Van Mierlo, Novel thermal management methods to improve the performance of the Li-ion batteries in high discharge current applications, Energy (2021), 120165.
[12] Z. Wang, H. Zhang, X. Xia, Experimental investigation on the thermal behavior of cylindrical battery with composite paraffin and fin structure, Int. J. Heat Mass Transf. 109 (2017) 958–970.
[13] G. Jiang, J. Huang, M. Liu, M. Cao, Experiment and simulation of thermal management for a tube-shell li-ion battery pack with composite phase change material, Appl. Therm. Eng. 120 (2017) 1–9.
[14] S. Lei, Y. Shi, G. Chen, A lithium-ion battery-thermal-management design based on phase-change-material thermal storage and spray cooling, Appl. Therm. Eng. (2020) 168.
[15] F. Zhang, L. Zhai, L. Zhang, M. Yi, B. Du, S. Li, A novel hybrid battery thermal management system with fins added on and between liquid cooling channels in composite phase change materials, *Appl. Therm. Eng.,* 207, 118198.
[16] P. Ping, R. Peng, D. Kong, G. Chen, J. Wen, Investigation on thermal management performance of PCM-fin structure for Li-ion battery module in high-temperature environment, Energ. Conver. Manage. 176 (2018) 131–146.
[17] K. Ramin, B. Kamkari, Investigation of the effect of inclination angle on the melting enhancement of phase change material in finned latent heat thermal storage units, Appl. Therm. Eng. 146 (2019) 45–60.
[18] R. Widyantara, M. Naufal, P. Sambegoro, I. Nurprasetio, F. Triawan, D. Djamari, A. Nandiyanto, B. Budiman, M. Aziz, Low-cost air-cooling system optimization on battery pack of Electric Vehicle, Energies 14 (2021) 7954.
[19] P. Qin, J. Sun, X. Yang, Q. Wang, Battery thermal management system based on the forced-air convection: A review, eTransportation 7 (2021), 100097.
[20] W. Li, A. Jishnu, A. Garg, M. Xiao, X. Peng, L. Gao, Heat transfer efficiency enhancement of lithium-ion battery packs by using novel design of herringbone fins, J. Electrochem. Energy Convers. Storage 17 (2) (2020).
[21] W. Chen, S. Hou, J. Shi, P. Han, B. Liu, B. Wu, X. Lin, Numerical analysis of novel air-based Li-ion battery thermal management, Batteries 8 (9) (2022) 17.
[22] Y. Xu, H. Zhang, X. Xu, X. Wang, Numerical Analysis and surrogate model optimization of air-cooled battery modules using double-layer heat spreading plates, Int. J. Heat Mass Transf. (2021), 121380.
[23] A.K. Thakur, R. Prabakaran, M. Elkadeem, S. Sharshir, M. Arıcı, C. Wang, W. Zhao, J.-Y. Hwang, R. Saidur, A state of art review and future viewpoint on advance cooling techniques for Lithium–ion battery system of electric vehicles, J. Storage Mater. 32 (2020), 101771.
[24] Z. Zhang, E. Lau, C. Botting, M. Bahrami, Naturally cooled heat sinks for battery chargers, 147 (2020) 118911.
[25] W. Yang, F. Zhou, H. Zhou, Y. Liu, Thermal performance of axial air cooling system with bionic surface structure for cylindrical lithium-ion battery module, Int. J. Heat Mass Transf. 161 (2020), 120307.
[26] K.-H. Chen, T. Han, B. Khalighi, P. Klaus, Air cooling concepts for Li-ion battery pack in Cell Level, in: *Volume 1: Aerospace Heat Transfer; Computational Heat Transfer; Education; Environmental Heat Transfer; Fire and Combustion Systems; Gas Turbine Heat Transfer; Heat Transfer in Electronic Equipment; Heat Transfer in Energy Systems,* 2017.
[27] D. Chen, J. Jiang, G.-H. Kim, C. Yang, A. Pesaran, Comparison of different cooling methods for lithium ion battery cells, Appl. Therm. Eng. 94 (2016) 846–854.
[28] Q. Gao, Y. Yan, Y. Yuying, G. Wangg, Thermal management optimization of a lithium-ion battery module with graphite sheet fins and liquid cold plates, Autom. Innov. 3 (4) (2020) 336–346.
[29] S.K. Mohammadian, S.M. Rassoulinejad-Mousavi, Y. Zhang, Thermal management improvement of an air-cooled high-power lithium-ion battery by embedding metal foam, J. Power Sources 296 (2015) 305–313.
[30] K.S. Mohammadian, Y. Zhang, Cumulative effects of using pin fin heat sink and porous metal foam on thermal management of lithium-ion batteries, Appl. Therm. Eng. 118 (2017) 375–384.
[31] S. Mohammadian, Y. Zhang, Thermal management optimization of an air-cooled li-ion battery module using PIN-fin heat sinks for hybrid electric vehicles, J. Power Sources 273 (2015) 431–439.
[32] L. Cheng, A. Garg, A. Jishnu, L. Gao, Surrogate based multi-objective design optimization of lithium-ion battery air-cooled system in electric vehicles, J. Storage Mater. 31 (2020), 101645.
[33] R. Zhao, D. Wen, Z. Lai, W. Li, M. Ye, W. Zhuge, Y. Zhang, Performance analysis and optimization of a novel cooling plate with non-uniform pin-fins for lithium battery thermal management, *Appl. Therm. Eng.,* 194 (2021) 117022.
[34] zhangleiytu, The differences between lithium cylindrical and prismatic cells, 2023. [Online]. Available: https://www.evlithium.com/Blog/difference-between-cylindrical-and-prismatic-cells.html.
[35] A. Saeed, N. Karimi, M.C. Paul, Analysis of the unsteady thermal response of a Li-ion battery pack to dynamic loads, Energy 231 (2021), 120947.
[36] H. Wang, Y. Wang, F. Hu, W. Shi, X. Hu, H. Li, S. Chen, H. Lin, C. Jiang, Heat generation measurement and thermal management with phase change material based on heat flux for high specific energy power battery, Appl. Therm. Eng. 194 (2021), 117053.
[37] K. Chen, Y. Chen, Y. She, S. Wang, L. Chen, Construction of effective symmetrical air-cooled system for Battery Thermal Management, Appl. Therm. Eng. 166 (2020), 114679.
[38] Effect analysis on thermal profile management of a cylindrical lithium-ion battery utilizing a cellular liquid cooling jacket, *Energy,* (2021) 119725.

[39] L. Sheng, Z. Zhang, L. Su, H. Zhang, H. Zhang, K. Li, Y. Fang, W. Ye, A calibration calorimetry method to investigate the thermal characteristics of a cylindrical lithium-ion battery, Int. J. Therm. Sci. 165 (2021), 106891.
[40] V. Choudhari, A. Dhoble, S. Panchal, M. Fowler, R. Fraser, Numerical investigation on thermal behaviour of 5 × 5 cell configured battery pack using phase change material and fin structure layout, J. Storage Mater. 43 (2021), 103234.
[41] H.-W. Wu, Y.-C. Ciou, J.-K. Wu, Study of natural convection of lithium-ion battery module employing phase change material, Processes 9 (11) (2021) 2023.
[42] T.-H. Shih, W. Liou, A. Shabbir, Z. Yang, J. Zhu, A new K-∈ Eddy viscosity model for high Reynolds number turbulent flows, Comput. Fluids 24 (3) (1995) 227–238.
[43] M. Li, F. Liu, B. Han, J. Guo, Y. Xu, Research on temperature control performance of battery thermal management system composited with multi-channel parallel liquid cooling and Air Cooling, Ionics 27 (6) (2021) 2685–2689.
[44] L. Fezoui, B. Stoufflet, A class of implicit upwind schemes for Euler simulations with unstructured meshes, J. Comput. Phys. 84 (1) (1989) 174–206.
[45] S. Patankar, Numerical Heat Transfer and Fluid Flow, Hemisphere Publishing, New York, 1980.
[46] W. Lu, Z. Liu, J.-F. Flor, Y. Wu, M. Yang, Investigation on designed fins-enhanced phase change materials system for thermal management of a novel building integrated concentrating PV, Appl. Energy 225 (2018) 696–709.